ADVANCES IN AGRICULTURAL AND FOOD RESEARCH JOURNAL

Original Research Article

Comparative Analysis of UAV and TLS-Derived Crown and Frond Data for Detecting Basal Stem Rot in Oil Palms

Nur Azuan Husin [1,2,3]*, Nurul Izzah Zainal Abidin [1], Siti Khairunniza-Bejo [1,2,3]

[1]Smart Farming Technology Research Centre, Universiti Putra Malaysia, 43400 UPM Serdang, Selangor, Malaysia. nurazuan@upm.edu.my

[2]Department of Biological and Agricultural Engineering, Faculty of Engineering, Universiti Putra Malaysia, 43400 UPM Serdang, Selangor, Malaysia. skbejo@upm.edu.my

3 Laboratory of Plantation System Technology and Mechanization (PSTM), Institute of Plantation Studies, Universiti Putra Malaysia, Serdang 43400, Malaysia

*Corresponding author: Nur Azuan Husin, Department of Biological and Agricultural Engineering, Faculty of Engineering, Universiti Putra Malaysia, 43400 UPM Serdang, Selangor, Malaysia; nurazuan@upm.edu.my

Abstract: Basal Stem Rot (BSR) disease, caused by *Ganoderma boninense*, is one of the most destructive diseases affecting oil palm plantations in Southeast Asia. Traditional detection methods are invasive, time-consuming, and often ineffective during the early stages of infection. This study evaluates the effectiveness of Unmanned Aerial Vehicle (UAV) imagery compared with Terrestrial Laser Scanning (TLS) for detecting BSR disease through structural canopy features. Three canopy features: crown area, frond number, and frond angle were extracted from UAV top-view imagery and TLS point-cloud data. Forty oil palm trees were assessed, with ten trees representing each of four disease severity levels: healthy (T0), early infection (T1), moderate infection (T2), and severe infection (T3). Data from both platforms (UAV and TLS) were processed using image segmentation and evaluated using descriptive statistics, correlation analysis (r and R^2), Root Mean Square Error (RMSE) and inferential statistics. UAV and TLS measurements showed strong correlations, particularly for frond number (r = 0.993, R^2 = 0.98) and frond angle (r = 0.999, R^2 = 0.99 in moderate infection). ANOVA confirmed significant differences among disease severity levels for all canopy features ($p < 0.0001$). Paired t-tests indicated no significant differences between UAV and TLS for frond number and frond angle in moderate and severe infections, while significant differences occurred in healthy and early-stage palms due to canopy density and occlusion. Crown area remained significantly different across most severity levels, reflecting segmentation limitations in UAV imagery. Overall, the findings demonstrate that UAV imaging is a scalable and cost-effective tool for plantation-wide BSR monitoring, while TLS remains valuable as a high-resolution reference method.

Keywords: *Ganoderma boninense*; UAV; Terrestrial Laser Scanning (TLS); Remote Sensing

Received: 9th June 2025

Accepted: 3rd December 2025

Available Online: 8th January 2026

Published: 29th April 2026

Citation: Husin, N. A., Zainal Abidin, N. I., Khairunniza-Bejo, S. Comparative analysis of UAV and TLS-derived crown and frond data for detecting basal stem rot in oil palms. *Adv Agri Food Res J* 2026; 7(1): a0000628. https://doi.org/10.36877/aafrj.a0000628.

1. Introduction

Oil palm (*Elaeis guineensis*) is a major economic crop in Malaysia, contributing significantly to the country's Gross Domestic Product (GDP) through substantial global production and export percentages. Despite its economic importance, oil palm plantations face serious threats from Basal Stem Rot (BSR) disease. BSR is responsible for severe yield losses, early tree mortality, and increased replanting costs, which directly impact the profitability and sustainability of the industry. BSR disease caused by the *Ganoderma boninense* (*G. boninense*) fungus is categorised as a soil-borne pathogen. Soil-borne pathogen lives within the soil, causing root disease that quickly spreads to other plant tissues and organs (Moura *et al*., 2022). Therefore, the keys to controlling this destructive disease are detection and diagnosis at an early stage.

In Malaysia, it was expected that over 60 million mature oil palms may become infected, showing 50% losses and 80% of stands died by the time the palms were 25 years old, with an estimated $365 million in economic losses annually (Siddiqui *et al*., 2021). The creation of successful disease control and plantation management needs to define the route of infection and the degree of pathogen diversity. Detection delays have been caused by the uncertainty between *Ganoderma zonatum*, the oil palm weak pathogen, and *G. boninense,* the major pathogen (Karunarathna *et al*., 2024). The belief that sexual reproduction plays an important role in the epidemiology of basal stem rot disease was supported by the high intraspecific variability found among *G. boninense* isolated from either neighbouring or distant trees. Another explanation is that the infection was not well-detected because the cycle consists of a variety of alternate and consecutive events in its early stages.

The symptoms of infected oil palm trees are detected visually on the leaf (foliar), stem, or trunk. The foliar symptoms of infected trees are similar hanging or drooping of the crown, a high presence of unopened spears, a smaller size of the palm’s crown and a decreasing number of the palm’s fronds. Traditional methods for detecting BSR, such as visual inspections and manual surveys, are often labour-intensive, time-consuming, and may lack accuracy, especially during the early stages of infection and sometimes confusing due to individual perceptions (Haw *et al*., 2023). To confirm the infection, laboratory analysis must be carried out further on the trunk samples. The drilling of the palm trunk would possibly damage the trees and should be avoided. Moreover, these approaches can be invasive, potentially causing additional stress to the trees. This indicates the need to establish a more convenient method for recognising BSR diseases.

In response to these challenges, advancements in remote sensing technologies have introduced non-destructive alternatives for disease detection. Remote sensing technologies have transformed agricultural monitoring by providing non-invasive methods for assessing plant health. In oil palm plantations, techniques such as hyperspectral imaging, multispectral imaging, and LiDAR-based terrestrial laser scanning (TLS) have been employed to detect BSR disease with high degrees of success (Husin *et al*., 2020b; Azuan *et al*., 2019). TLS offers detailed three-dimensional (3D) structural data of individual trees, facilitating the analysis of canopy architecture, including crown area, frond number, and frond angle, which are crucial indicators of BSR infection (Husin *et al*., 2020a; Husin *et al*., 2020c). Even though TLS is a ground-based scanner, using a multi-scan approach around the target (oil palm tree) and a combination of point clouds allows for virtual navigation, including top-down perspectives of the canopy. Studies have demonstrated that TLS can effectively classify disease severity levels based on structural changes in the canopy, although its application is limited by high initial costs, slow data acquisition, time-consuming data processing and the need for individual tree scanning. (Husin *et al*., 2021).

In contrast, Unmanned Aerial Vehicles (UAVs) or also known as drones, have emerged as an efficient tool for large-scale monitoring. UAV-based aerial imagery enables rapid data collection over vast plantation areas, making it ideal for frequent monitoring (Liu *et al*., 2021). The UAVs equipped with high-resolution cameras can capture top-view images that can be analysed for canopy health indicators such as crown area and frond features (Yarak *et al*., 2021). Studies have shown that UAVs could be employed to detect changes in the aerial view of the canopy for early detection of BSR disease (Kent *et al*., 2023; Kurihara *et al*., 2022).

However, no studies have directly compared TLS and UAV-derived features such as crown area, frond number and frond angle for BSR detection in oil palm plantations. This study aims to compare UAV and TLS-derived crown and frond data for detecting BSR in oil palms. By evaluating the accuracy and reliability of UAV data against ground-based LiDAR (TLS) measurements, this research seeks to validate UAV as a viable large-scale monitoring tool for BSR detection, thereby informing better management practices and mitigating the adverse effects of BSR on oil palm cultivation.

2. Materials and Methods

2.1 Study Area

The study area was located in Seberang Perak, Malaysia (Figure 1) (4°08'04.6"N 100°55'04.3" E). The replanted plantation area's oil palm trees were all about 10 years old, which is when palm oil yield peaks. The trees were bred from D x P (*Dura*×Psifera) and were planted in peat soil. The study field had a topology with a slope variation of less than one degree and an average elevation of 19.36 m above sea level. In terms of fertilisation, fruit harvesting, trimming, and weed control, the oil palm plantation was maintained in the same

state as commercial oil palm farms. Pruning mature palms was conducted as scheduled to get rid of senescing or dead leaves and make it possible to reach the FFBs at the right time for harvest. The plantation has palms spaced 9×9×9 m^3 apart in an equilateral triangular pattern and has a planting density of 142 palms per hectare. Four severity categories were used to categorise the oil palm trees, both infected and uninfected: healthy (T0), initially infected (T1), moderately infected (T2), and severely infected (T3). These oil palm tree severity ratings will determine the outcome and future conversations. Experts from the Malaysian Oil Palm Board (MPOB) assessed the categories of BSR infection in trees based on visual symptoms, as shown in Table 1. The sampling followed a completely randomised design (CRD) where 40 palms (replication of 10 trees per severity level) were selected randomly within the same plot. The response variables measured were: (i) crown area, (ii) frond number, and (iii) frond angle.

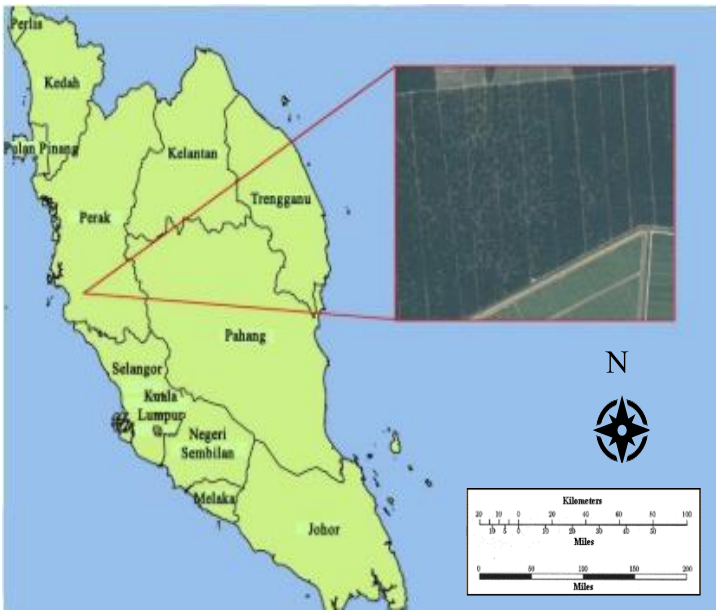

Figure 1. Location of the study site at Seberang Perak, Malaysia

Table 1. BSR disease categories with their description

Severity Score	Severity Levels	Grouping Symptoms
T0	Healthy	No disease symptoms are visible on the tree (top or bottom)
T1	Early Infection	Still capable of producing fruit, healthy frond or 1–3 unopened spear frond but Ganoderma fruiting body appears at the bottom trunk
T2	Moderate Infection	Still capable of producing fruit with 3–6 unopened spear fronds and 50% or more frond canopy start to bend down, few leaves start yellowing, and Ganoderma fruiting body appears
T3	High Infection	No more fruit produced, with dried and rotting frond at palm base, small canopy, and Ganoderma fruiting body appears

2.2 UAV Data Collection

Aerial photographs of an oil palm plantation in Seberang Perak, Malaysia, were used as UAV input for this study. The aerial photographs were acquired from a standard drone, Mavic 2 Pro, with a digital camera (RGB) to produce the aerial data. The drone flew 120 m above the oil palm plantation with a resolution of 20 MP. The drone has a maximum flight distance of 18 km (at a consistent 50 kph), 31 min max flight time (at a consistent 25 kph), battery capacity of 3850 mAh and can fly at a maximum of 6000 m altitude. The integrated camera is a Hasselblad L1D-20c camera (Hasselblad Group, Göteborg, Sweden), which has a 20 MP CMOS sensor (5472×3648 pixels), the optical parameters at a nominative focal length of 10.3 mm and an optical aperture of f/2.8. The data extracted from the high-resolution top-view aerial images gathered were compared with the TLS data from the same study area. The orthophoto mosaic image obtained (Figure 2a) was used to extract the top-view features, such as crown pixel, frond numbers, and frond angle for each of the oil palm trees in the oil palm plantation for *G. Boninense* disease detection.

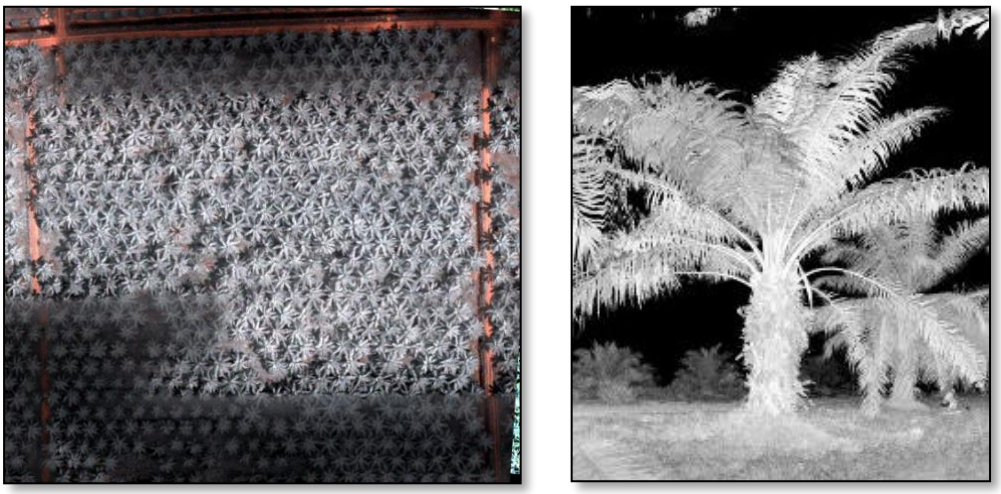

(a) **(b)**

Figure 2. (**a**) Orthophoto mosaic image from the drone, (**b**) Overview of point cloud image from TLS

2.3 TLS Data Collection

TLS data were collected using a FARO Focus 3D X 120 laser scanner (FARO Technologies, Inc., Lake Mary, USA), which operates on a continuous wave (phase-based) laser system with a wavelength of 905 nm in the mid-infrared spectrum. The resulting point cloud data were processed using FARO's SCENE software (FARO Technologies, Inc., Florida, USA), designed specifically for efficient handling and processing of scan data. The scanner features a maximum range of 120 m and a pulse repetition rate of 97 Hz, enabling it to rapidly capture millions of 3D data points with high precision. It functions by emitting an infrared laser beam directed through a rotating mirror, with reflected signals from object surfaces forming a 3D spatial point cloud. The scanner’s beam divergence was 0.27 mrad,

translating to a 27 mm beam expansion per 100 m. Its field of view spans 360° horizontally and 305° vertically, constrained only by the scanner base. Multiple scan positions were aligned using the registration function in SCENE to generate a unified point cloud dataset (see example in Figure 2b). Individual oil palm trees were isolated for analysis using a clipping box during the preprocessing stage. Each tree was scanned from 4 positions arranged around the palm to minimise occlusion, with an average scanning distance of 1.5 m from the trunk.

2.4 Data Processing

2.4.1 UAV images processing

Orthorectified images of the study area were initially generated and subsequently processed through a series of segmentation and object analysis techniques. The full orthomosaic image was assembled using QGIS software (version 3.10), providing a comprehensive view of the entire study site. Individual oil palm crowns were then extracted by cropping the mosaic using Microsoft Paint (Microsoft Corp., Redmond, USA), isolating each tree for further analysis in MATLAB. To separate the crown region from its background, Otsu's threshold segmentation method was employed. First, the RGB images were converted to grayscale using the rgb2gray function. These grayscale images were then binarised using the "graythresh" function, which applies Otsu's method to determine an optimal threshold value. Pixels with intensities above the threshold were assigned a value of "1" (white), and those below were assigned "0" (black), resulting in a binary image. This process effectively isolated the crown area by identifying connected regions of white pixels. The crown area was then quantified using the "bwarea" function, which calculates the total area of white pixels in the binary image.

The same images were used for determining frond number and frond angle. To delineate individual fronds, polylines were manually traced over the binary crown image following the shape of visible fronds, as illustrated in Figure 3. Fronds that were overlapped or obscured beneath others in the top-down view were excluded from analysis. The total frond number was determined by counting the drawn polylines. Frond angle measurements were conducted using MATLAB's "bwtraceboundary" function, which traces the boundaries of binary objects. To simplify edge detection, each frond of interest was isolated by cropping the original image. An initial boundary point was specified to begin tracing, and the angle between each adjacent frond was calculated sequentially. This process was repeated until all visible frond angles were measured. In summary, both frond count and frond angle were derived from the segmented crown image using a combination of manual tracing and automated boundary analysis.

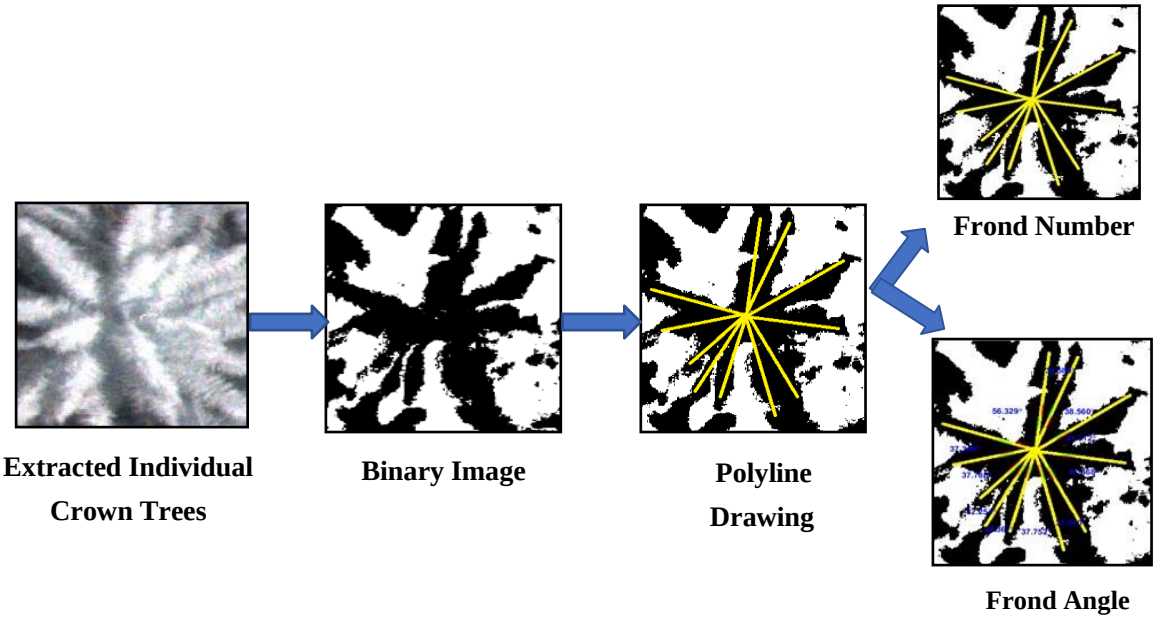

Figure 3. Frond metrics extracted from UAV oil palm images

2.4.2 TLS images processing

The number of pixels inside the crown image was used to calculate the crown area for each tree. The crown image, which was saved in JPEG format, was used in a top-down view. To ensure uniformity, the picture was cropped to 10 x 10 m so that the whole crown area was covered. After cropping the image with Paint software (Microsoft Corp., Redmond, USA) to eliminate extraneous elements like fronds from other trees, MATLAB software (Mathworks Inc., Natick, USA) was used for further processing. The crown image was extracted from the background using Otsu's algorithm. The same top-down image of the oil palm crown was utilised for both frond counting and frond angle measurement. The image was imported into AutoCAD software (Autodesk, Inc., San Rafael, USA) for analysis. A new layer was created using the "layers" feature and set as the active working layer. Using the "draw" tool and the "polyline" function, each visible frond was manually traced based on its shape as seen in the 2D image. Only fronds clearly visible from the top view were included; any fronds obscured beneath others or overlapping were excluded. The same image was then used to measure the angles between fronds. The "dimension" tool was applied to calculate the angle between adjacent fronds, capturing the spacing distribution across the canopy. This process was repeated for all visible fronds on each tree.

2.4.3 Descriptive statistics analysis

To assess the reliability of UAV-derived measurements against TLS ground data, both bar chart visualisation and correlation analysis were employed. Bar charts were used to illustrate the comparative trends of structural features, namely frond number, frond angle, and crown area, across four disease severity categories: healthy (T0), early infected (T1), moderately infected (T2), and severely infected (T3). These charts allowed for clear visual

interpretation of how each parameter varied with increasing infection severity and how closely UAV measurements followed TLS data patterns. In addition to visual comparison, Pearson correlation coefficients and R-squared (R^2) values were calculated to quantify the strength and linearity of the relationship between TLS and UAV-derived measurements. High correlation values across most parameters confirmed the consistency between both sensing platforms, while Root Mean Square Error (RMSE) metrics were computed to evaluate absolute differences. Together, the bar charts and correlation analyses provided both qualitative and quantitative validation of UAV performance in replicating TLS-derived canopy features, reinforcing its potential as a scalable tool for BSR monitoring in oil palm plantations. In addition, Figure 4 below illustrates the flowchart of the methods used in this study.

2.4.4 Inferential statistical analysis

To evaluate differences in structural canopy features across disease severity levels and between sensing platforms, inferential statistical tests were performed. First, a one-way ANOVA was applied separately to the TLS and UAV datasets to determine if crown area, frond number, and frond angle varied significantly among the four BSR severity categories (T0 to T3). This analysis identifies statistically detectable changes in canopy structure associated with disease progression. Next, paired *t*-tests were used to assess the agreement between TLS and UAV measurements within each severity class, revealing any significant discrepancies between UAV-derived and TLS-derived values for each canopy feature. A significant level of $p < 0.05$ was used for all tests. The ANOVA captured overall structural differences across disease stages, while the paired *t*-tests provided feature-specific evaluations of UAV-TLS measurement consistency. Together, these analyses quantify both the biological separation of severity levels and the operational accuracy of UAV relative to TLS. All statistical analyses were conducted in JMP (Trial version 18.0.1, SAS Institute Inc., Cary, NC, USA).

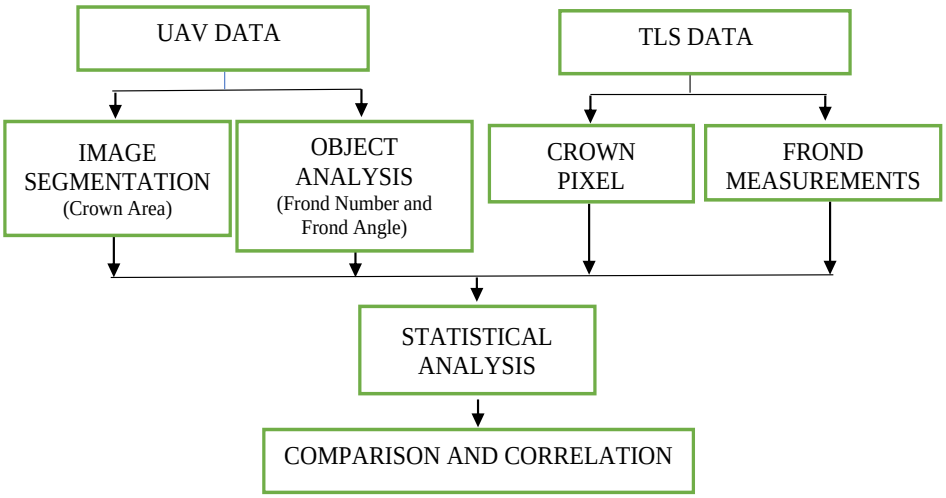

Figure 4. Flowchart of methods

3. Results and Discussions

3.1. Analysis of Frond Number

The results presented in Figure 5 illustrate a clear comparative trend between the frond number data extracted using TLS and UAV imagery for four levels of BSR severity: T0 (healthy), T1 (early), T2 (moderate), and T3 (severe). Both TLS and UAV datasets demonstrate a consistent decreasing pattern in frond number across increasing BSR severity levels, which supports the hypothesis that disease progression affects canopy structure. For TLS data, the mean frond number for healthy trees (T0) was the highest, while severely infected trees (T3) showed a substantial reduction. Similar trends are observable in maximum and minimum values, indicating not only a reduction in average frond count but also a constriction in canopy variation among more severely infected palms. UAV-derived data followed a comparable trend, though the differences between severity levels appear less pronounced, particularly between T2 and T3.

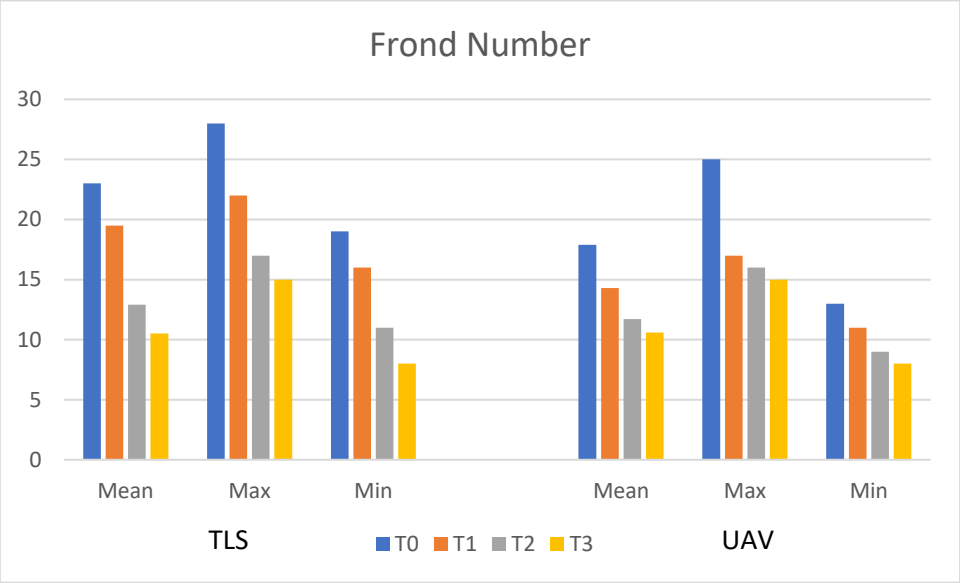

Figure 5. Graph of mean, maximum and minimum of frond number in T0 to T3 categories for TLS and UAV data

The slightly higher values in TLS-derived frond counts-especially for T0 and T1, suggested a higher resolution and accuracy in capturing complex canopy structures using ground-based scanning. TLS systems, with their dense point clouds and full 3D reconstruction capabilities, are more effective in penetrating through overlapping fronds and accounting for subtle variations in frond orientation and coverage. Conversely, UAV imagery, despite offering wide coverage and faster data acquisition, is more susceptible to occlusion and under-detection, particularly for downward-facing or shaded fronds. However, UAV-based analysis showed reasonable approximation to TLS data, especially in terms of mean and maximum values for early-stage infections (T0 and T1), which are critical for early detection efforts. The convergence of data in these categories indicates the feasibility of UAV

imaging for operational-scale disease monitoring, particularly where TLS deployment is restricted due to cost or terrain limitations.

The correlation analysis (Figure 6) further supports the reliability of UAV-based frond number estimation when compared against the TLS data. Across all four severity levels (T0 to T3), the Pearson correlation coefficient (r) and coefficient of determination (R^2) values were notably high, indicating strong linear relationships between the frond numbers extracted via TLS and UAV methods. Healthy palms (T0) exhibited the strongest correlation (R^2 = 0.98), followed closely by severely infected palms (T3) with R^2 = 0.98. This suggests that both severe infections, where canopy structures were either fully intact or significantly reduced, were most consistently captured by both UAV and TLS systems. Early (T1, r = 0.9629, R^2 = 0.93) and moderately (T2, r = 0.9554, R^2 = 0.91) infected trees displayed slightly lower, yet still robust correlations. These findings indicated that the UAV approach can effectively simulate TLS results in quantifying frond-based structural features, particularly in early (T0, T1) and late (T3) stages of infection. The consistency of UAV estimates across these groups highlights its potential for timely disease detection and classification, a crucial factor in integrated pest management strategies within large-scale plantations. Moreover, the strong correlation across severity levels implied that crown and frond features were stable indicators for differentiating disease stages. This validated the use of UAV-derived structural parameters in developing predictive models for BSR progression.

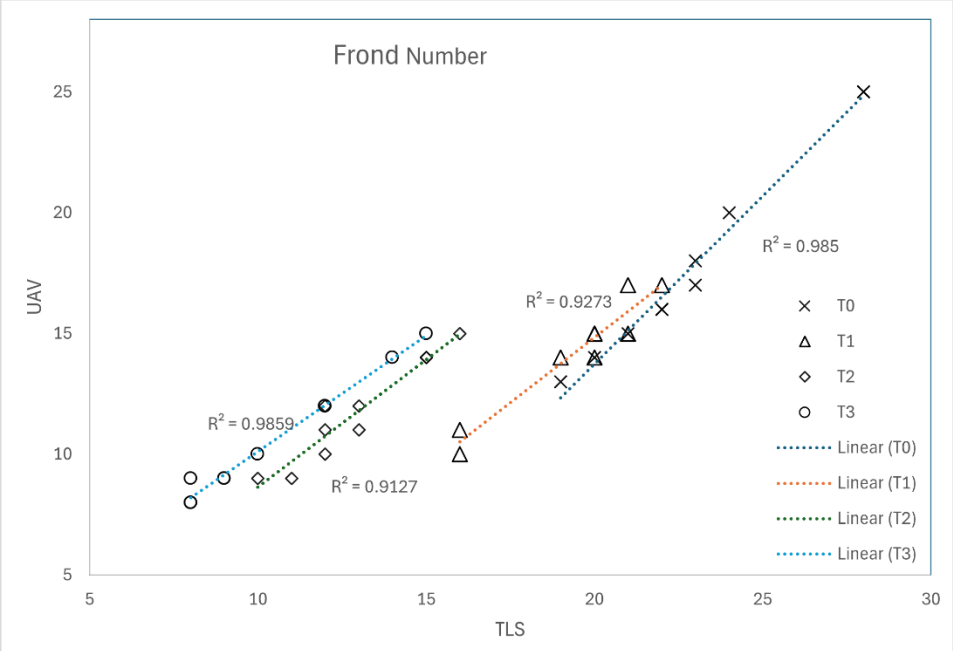

Figure 6. Correlations of frond number for UAV and TLS

Interestingly, the RMSE values revealed an inverse trend. While the correlation remains high in T0 and T1, the corresponding RMSE values (27.5 and 27.4, respectively) were significantly higher than those for T2 and T3 (1.8 and 0.1, respectively). This indicated

that although the general trend between UAV and TLS measurements was consistent, UAV-based estimations for healthy and early infected trees may deviate more in absolute terms. This disparity can be attributed to the structural complexity of healthy and early-stage infected canopies. Dense frond arrangements and overlapping structures in T0 and T1 trees can increase the likelihood of underestimation when captured from a nadir UAV perspective. In contrast, frond loss and crown thinning in T2 and T3 trees enhance visibility, thereby reducing error and improving alignment with TLS data. These findings highlight the strengths of UAV systems in detecting advanced infection stages but also underscore their limitations in early detection. Improved image segmentation techniques or the integration of oblique imagery may help reduce RMSE and enhance UAV effectiveness for early-stage disease surveillance. Overall, the combination of high correlation and low RMSE in T2 and T3 supports UAV's potential as a reliable remote sensing tool in precision agriculture.

3.2 Analysis of Frond Angle

The comparison of frond angle data between TLS and UAV methods (Figure 7) revealed distinct patterns related to the progression of *G.boninense* infection in oil palm trees. Both technologies demonstrated a general increase in mean, maximum, and minimum frond angles as disease severity intensified from T0 (healthy) to T3 (severely infected). For TLS data, the mean frond angle gradually increased from T0 to T3, with the maximum angle showing a substantial jump, particularly in T3 trees, where frond drooping is most pronounced. This trend is expected, as advanced BSR infection typically results in the weakening of frond attachment and reduced structural rigidity, causing fronds to hang at wider angles. Notably, TLS captured the most extreme angles (up to ~53° for T3), reflecting its ability to model subtle spatial variations in canopy geometry.

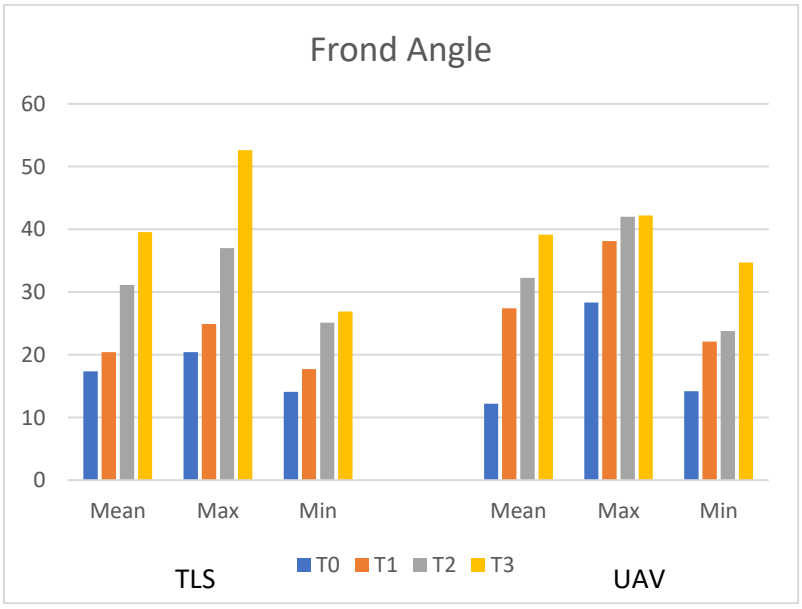

Figure 7. Graph of mean maximum and minimum of frond angle in T0 to T3 categories for TLS and UAV data

UAV-based measurements also showed a rising trend in frond angles with increasing disease severity, particularly in the maximum and mean values. However, in contrast to TLS, UAV estimations for T0 and T1 exhibited more variance and potential overestimation, possibly due to challenges in detecting shallow or overlapping fronds from a vertical perspective (Husin *et al*., 2020c). Nonetheless, the alignment of T2 and T3 values between TLS and UAV indicated that UAV imaging is more accurate in capturing frond behaviours in later disease stages where canopy openness improves visibility (Husin *et al*., 2022). The widening gap in minimum angles across severity levels may also provide useful classification indications. T3 palms showed the largest spread between maximum and minimum angles in both TLS and UAV data, reflecting the irregular positioning of surviving fronds in late-stage infections.

The correlation between TLS and UAV-derived frond angles, as depicted in Figure 8, reveals a consistently strong linear relationship across all four disease severity levels. The coefficient of determination (R^2) values are particularly high: T0 (r = 0.9726, R^2 = 0.94), T1 (r = 0.9805, R^2 = 0.96), T2 (r = 0.9999, R^2 = 0.99), and T3 (r = 0.9219, R^2 = 0.84). These results provide compelling evidence that UAV-based frond angle measurements closely align with ground-based TLS data, especially in moderately infected trees (T2), which displayed a high correlation. The high linearity observed in T2 palms (r = 0.9999, R^2 = 0.99) may reflect the structural uniformity of moderately diseased trees, where partial canopy decline enhances frond visibility without excessive deformation. Meanwhile, healthy (T0) and early infected (T1) palms also demonstrated high correlation values, underscoring the ability of UAV systems to accurately detect angular differences in early-stage infections despite denser canopy structures. In contrast, the lowest correlations were recorded for severely infected palms (T3), with an r = 0.9219 and R^2 of 0.84. Despite the slight drop in T3 accuracy, the overall results affirm the effectiveness of UAV systems in estimating frond angles across health statuses. The alignment with TLS data further supports the viability of frond angle as a quantitative indicator for classifying BSR severity. This strengthens the case for UAV deployment in remote plantation monitoring, especially when integrated with other physical indicators such as crown area and frond number.

However, the RMSE analysis offers a complementary perspective on model accuracy. While T2 again shows the lowest RMSE (12.4), suggesting minimal deviation between UAV and TLS frond angles, T1 exhibited a notably high RMSE of 55.8 despite its high correlation. This discrepancy suggests that although the overall trends in frond angle variation were consistent (high correlation), the absolute UAV values for T1 deviated significantly from TLS measurements, possibly due to inconsistent segmentation during image processing. For T0 and T3, the RMSE values were 20.7 and 32.6, respectively. These moderate error levels may reflect structural complexities in healthy palms (T0), where denser frond arrangements hinder accurate UAV detection, and from the structural disintegration seen in T3 palms, as irregular frond collapse produces less predictable angular patterns. Altogether, the correlation and RMSE results suggest that UAV-based frond angle detection performs most reliably in

mid-stage disease severity (T2), where the canopy is sufficiently open for aerial visibility but not excessively deformed. In contrast, early (T1) and late (T3) stages pose greater challenges for UAV estimation due to either frond density or variability.

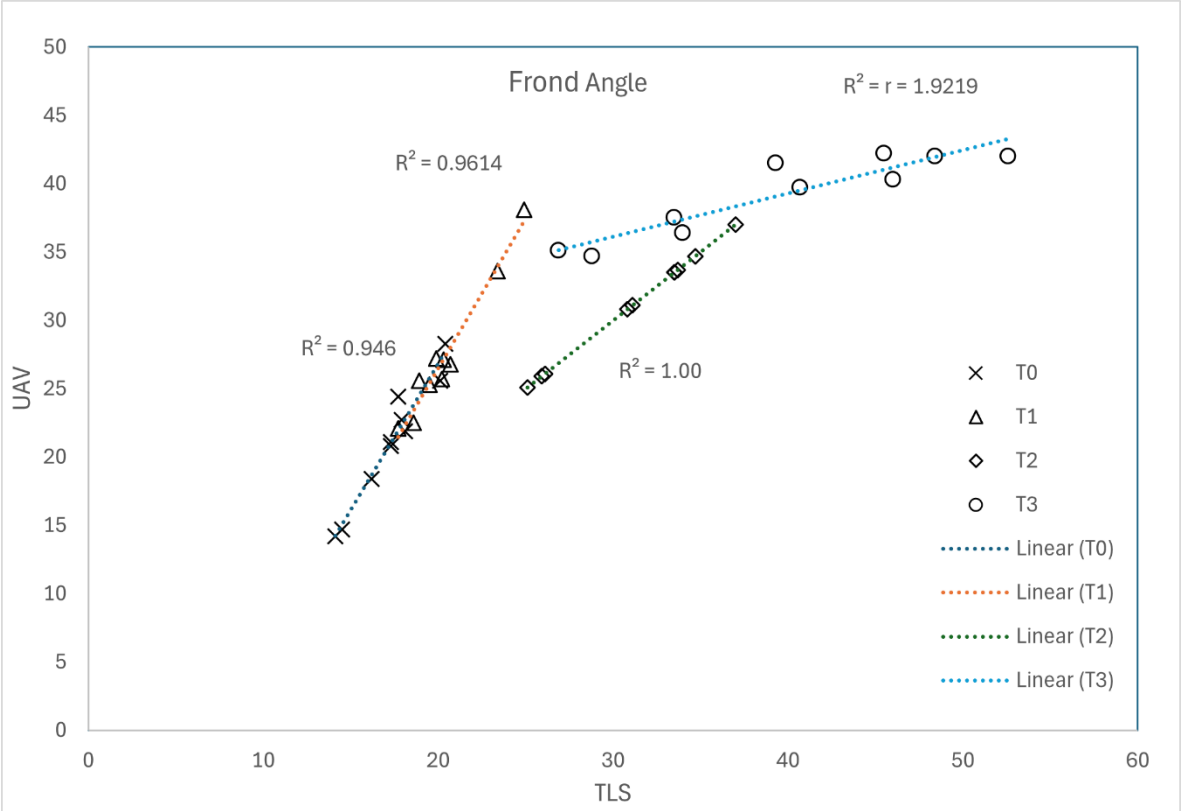

Figure 8. Correlations of frond angle for UAV and TLS

3.3 Analysis of Crown Pixel

The comparison of crown area values derived from TLS and UAV imagery (Figure 9) revealed a clear decreasing trend in canopy size with increasing severity of *G. boninense* infection. Both TLS and UAV systems consistently capture this decline across all statistical measures, mean, maximum, and minimum indicating the progressive structural impact of BSR on oil palm canopies. TLS-based crown area results showed that healthy palms (T0) and early infected palms (T1) maintain large and consistent canopy coverage, with mean values exceeding 85,000 pixels. In contrast, T2 and especially T3 palms exhibited a marked reduction, dropping below 70,000 and 65,000 pixels, respectively. This pattern aligns with known disease symptoms, as infected palms undergo frond loss and reduced photosynthetic area, leading to visibly smaller crowns.

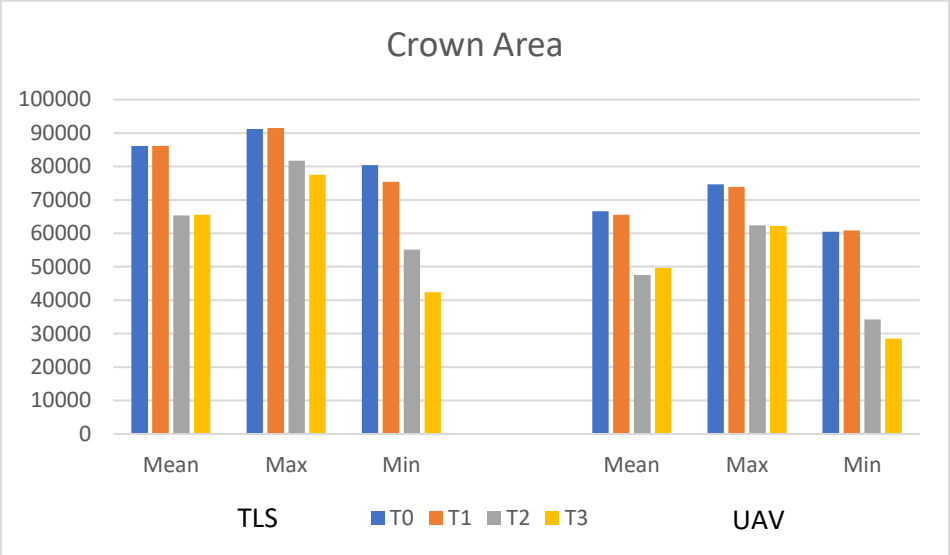

Figure 9. Graph of mean, maximum and minimum of crown area in T0 to T3 categories for TLS and UAV data

UAV-derived measurements displayed the same downward trend, though with slightly lower absolute values across all severity levels. Furthermore, UAV estimations for minimum crown area in T2 and T3 were noticeably lower than TLS, suggesting enhanced sensitivity to crown thinning in more severely affected trees. Despite these discrepancies, UAV-based results remain consistent in their ability to discriminate among severity levels. This suggests that UAV systems, even with partial visibility, are capable of capturing essential patterns in canopy structure indicative of disease progression. Furthermore, the TLS method demonstrates more efficacy in isolating individual tree crowns, primarily attributed to its advanced three-dimensional (3D) scanning capability. This technology enables penetration through multiple layers of branches, effectively capturing the intricate structures of the canopy. Conversely, the UAV method, despite its effectiveness in mapping larger areas, encounters challenges in distinguishing overlapping tree crowns. This limitation arises from its reliance on surface-level imagery acquired from an aerial perspective, which restricts its ability to discern the vertical complexity inherent in densely populated canopies.

The correlation analysis of crown area estimates between UAV and TLS systems (Figure 10) revealed a moderate to strong relationship across all BSR severity levels, though notably lower than correlations observed for frond number and frond angle. The correlation values demonstrated moderate to strong alignment with TLS-derived ground-based data, with T2 exhibiting the highest correlation (r = 0.9117, R^2 = 0.83), followed by T0 (r = 0.8609, R^2 = 0.74), T3 (r = 0.811, R^2 = 0.65), and T1 (r = 0.6685, R^2 = 0.44). These values indicate that while UAVs can approximate TLS crown area trends, variability exists particularly in early-stage infections. The relatively low correlation in T1 (r = 0.6685, R^2 = 0.44) was likely due to the subtle nature of early BSR symptoms, where minor reductions in crown density were not easily detected from a top-down UAV perspective. Overlapping fronds and dense

canopies in T0 and T1 may obscure the true crown boundary, leading to under-segmentation and reduced measurement accuracy. In contrast, the T2 group achieved the highest correlation (r = 0.9117, R^2 = 0.83), reaffirming that moderate canopy decline presents an optimal balance of visibility and structure for UAV detection. The highest correlation observed in T3 confirms that severe infection stages characterised by distinct canopy thinning and collapse (Husin *et al*., 2020b) were more easily captured from aerial perspectives. T0 also showed a strong correlation (r = 0.8609, R^2 = 0.74), suggesting that healthy and uninfected oil palm trees may still be distinguishable with UAV imaging, particularly when image quality and segmentation are optimised. While T3 palms display the most visible structural changes, their correlation value (r = 0.811, R^2 = 0.65) remains lower than T2. This may be due to inconsistencies in crown degradation among severely infected palms, where asymmetrical collapse and frond loss introduce irregularities that challenge automated image segmentation algorithms. To enhance UAV performance, advanced image processing techniques such as deep learning-based segmentation or oblique image capture could be explored to reduce crown underestimation, especially for healthy and densely foliated palms.

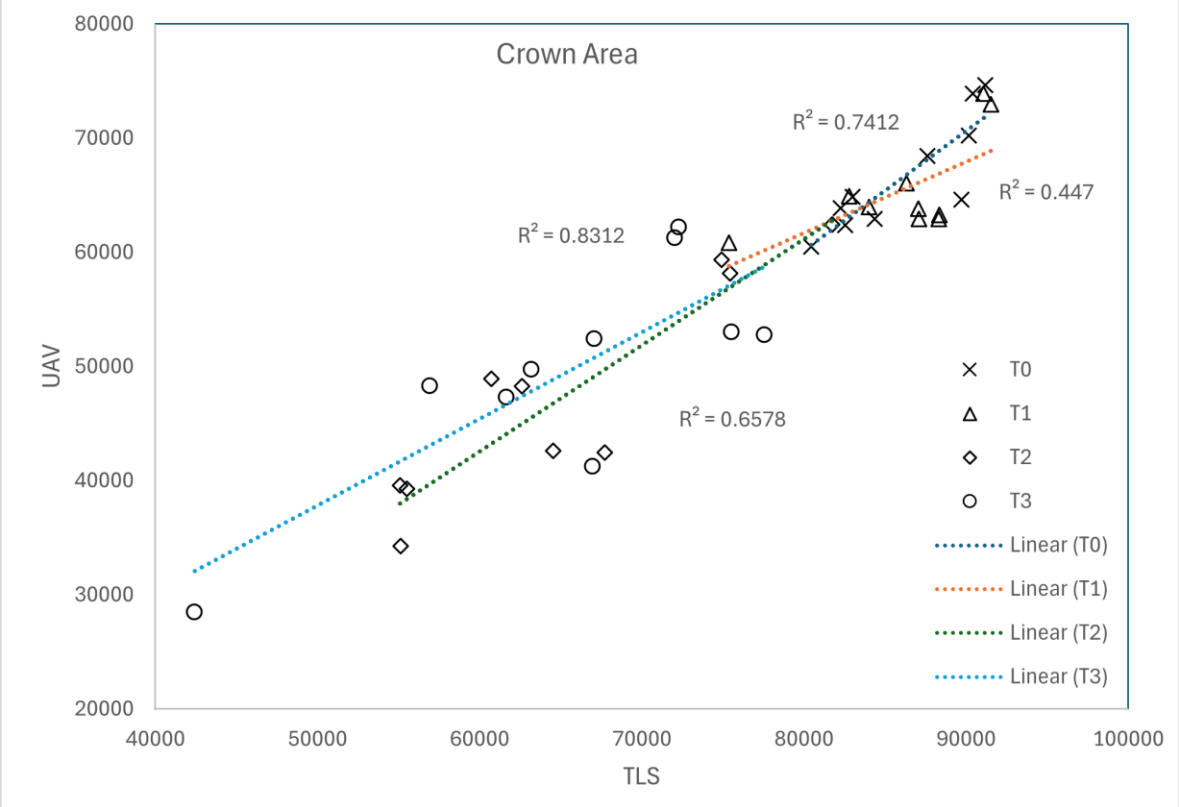

Figure 10. Correlations of crown area for UAV and TLS

The RMSE values reflected a similar trend, where all values remain in the order of magnitude of 10^8 pixels, while T3 produced the lowest RMSE (2.88×10^8). Conversely, T1 and T0 showed the highest RMSE values, 4.38×10^8 and 3.87×10^8, respectively. This inverse relationship, higher correlation with lower RMSE in advanced disease stages

supports the notion that UAV-based crown area estimation is more robust under conditions of significant canopy reduction. To mitigate these limitations in early detection, enhancements in UAV image resolution, multi-angle photogrammetry, or AI-based segmentation may be necessary. Nonetheless, crown area remains a valuable remote sensing indicator when interpreted within the context of other structural features and canopy conditions (Azuan *et al*., 2019; Husin *et al*., 2020a).

3.4 Analysis of variance (ANOVA) and T-test

The ANOVA results demonstrated highly significant differences (p-value < 0.0001) across all four BSR severity levels (T0 to T3) for both TLS and UAV datasets (Table 2). This supports the structural canopy parameters examined: frond number, frond angle, and crown area changed systematically as disease severity increases. These statistical outcomes are consistent with the descriptive findings, where healthy palms exhibited the highest frond counts, smallest frond angles and the largest crown areas, while severely infected palms showed pronounced frond loss, wider frond angles due to drooping, and significant canopy reduction. Thus, the ANOVA significance validates that these observable structural trends represent true biological differences associated with BSR progression.

Table 2. Results of ANOVA and T-test

Severity levels	Features	Paired t-test p-value (TLS vs. UAV)	One-way ANOVA p-value (TLS and UAV)
T0	Frond number	0.0067*	<0.0001*
	Frond angle	0.0290*	
	Crown pixel	<.0001*	
T1	Frond number	<.0001*	
	Frond angle	0.0013*	
	Crown pixel	<.0001*	
T2	Frond number	0.1995	
	Frond angle	0.6359	
	Crown pixel	0.0006*	
T3	Frond number	0.9311	
	Frond angle	0.8842	
	Crown pixel	0.0023*	

* Significant at 5% level

The paired t-tests provided insight into the agreement between TLS and UAV measurements within each severity category. For T0 (healthy) and T1 (early infection), the t-tests showed significant differences (p < 0.05) between the two platforms for all three features. This outcome aligns with descriptive findings showing that healthy and early infected canopies possess dense, overlapping fronds and minimal structural deformities. Such complexity creates occlusion in UAV top-view imagery, leading to underestimation of frond number, frond angle, and crown area when compared to TLS, which captures full 3D geometry without obstruction. These significant differences confirm that UAV faces limitations in early-stage detection where canopy structures remain compact and highly layered. In contrast, for T2 (moderate infection) and T3 (severe infection), the t-tests showed

no significant differences between TLS and UAV for frond number and frond angle, indicating much closer agreement between both platforms in later disease stages. This result corresponds well with the descriptive statistics, where frond loss and canopy thinning made fronds more visible from above, reducing occlusion and allowing the UAV to approximate TLS values more accurately. However, despite this convergence, crown area measurements remained significantly different ($p < 0.05$) even in T2 and T3. The crown areas become highly irregular in advanced infection due to asymmetric frond loss and crown collapse. These complex boundary changes explain why crown areas continue to show significant UAV-TLS differences across severity levels.

Overall, the combined analysis of frond number, frond angle, and crown area demonstrates a coherent structural response of oil palm canopies to increasing BSR severity, and collectively these features confirm the capability of UAV imaging to capture disease-related changes. While TLS remains the most precise method due to its detailed 3D reconstruction and ability to penetrate dense canopies, the results show that UAV measurements converge strongly with TLS in moderate and severe infection stages, where canopy openness improves visibility. More importantly, UAVs offer substantial operational benefits, including rapid coverage of large plantation areas, lower cost, minimal labour requirements, and non-destructive data collection, which makes them far more suitable for routine monitoring. Despite some limitations in dense, early-stage canopies, the overall findings support UAV technology as an effective and scalable tool for BSR surveillance, capable of providing reliable structural indicators for disease assessment when interpreted alongside TLS-validated trends.

4. Conclusion

This study demonstrated the effectiveness- of UAV-derived canopy features in assessing BSR infection in oil palm, using TLS measurements as the reference benchmark. By comparing three oil palm structural features - frond number, frond angle, and crown pixel across four severity levels, the study verified that UAV imagery can reliably reflect disease-related canopy changes and provide measurement outputs that align well with ground-based scanning. The statistical analyses further supported the consistency of UAV performance, particularly in conditions where canopy visibility improves and structural deformation becomes more pronounced. Beyond measurement accuracy, the broader value of UAV technology lies in its operational practicality. UAVs allow rapid data acquisition over wide areas, require minimal on-site labour, and offer a cost-efficient alternative to traditional field-based approaches. These advantages make UAVs far more suited for plantation-scale monitoring, where timely detection and repeated assessments are necessary for effective disease management. Future studies should evaluate multiple UAV flight altitudes (e.g., 60 m, 80 m, 120 m) to determine optimal resolution and canopy visibility for BSR detection. While TLS continues to serve as an important reference tool due to its high precision and detail, its deployment is limited by time, cost, and the need for close-range scans of individual

trees. The complementary strengths of both platforms reinforce the potential for integrated or hybrid approaches in future monitoring frameworks. Overall, the findings support UAV imaging as a reliable and scalable method for routine surveillance of oil palm health. With continued improvements in imagery processing, segmentation techniques, and automated classification models, UAV-based assessments can play a central role in supporting early intervention strategies and strengthening long-term BSR management across commercial plantation landscapes.

Author Contributions: Conceptualization, N.A.H.; methodology, N.A.H.; software, N.A.H.; validation, N.A.H.; formal analysis, N.A.H. and N.I.Z.A.; investigation, N.A.H. and N.I.Z.A.; resources, N.A.H. and S.K.-B.; data curation, N.A.H.; writing—original draft preparation, N.A.H. and N.I.Z.A; writing—review and editing, N.A.H., N.I.Z.A., and S.K.-B.; visualization, N.A.H.; supervision, N.A.H.; project administration, N.A.H.; funding acquisition, N.A.H.; All authors have read and agreed to the published version of the manuscript.

Funding: This research was funded by Malaysia Ministry of Higher Education (MOHE) and Universiti Putra Malaysia (UPM) under grant number GP-IPM/2021/9697200.

Acknowledgements: The author would like to thank all the supporting staff for their assistance and dedication throughout the implementation and execution of this study.

Conflicts of Interest: The authors declare no conflict of interest.

References

Azuan, N. H., Khairunniza-Bejo, S., Abdullah, A. F., *et al*. (2019). Analysis of changes in oil palm canopy architecture from basal stem rot using terrestrial laser scanner. *Plant disease, 103*(12), 3218–3225. https://doi.org/10.1094/PDIS-10-18-1721-RE

Haw, Y. H., Lai, K. W., Chuah, J. H., *et al*. (2023). Classification of basal stem rot using deep learning: a review of digital data collection and palm disease classification methods. *PeerJ Computer Science*, *9*, e1325. https://doi.org/10.7717/peerj-cs.1325

Husin, N. A., Bejo, S. K., Abdullah, A. F., *et al*. (2021). Relationship of oil palm crown features extracted using terrestrial laser scanning for basal stem rot disease classification. *Basrah Journal of Agricultural Sciences*, *34*, 1–10. https://doi.org/10.37077/25200860.2021.34.sp1.1

Husin, N. A., Khairunniza-Bejo, S., Abdullah, A. F., *et al*. (2020a). Classification of basal stem rot disease in oil palm plantations using terrestrial laser scanning data and machine learning. *Agronomy*, *10*(11), 1624. https://doi.org/10.3390/agronomy10111624

Husin, N. A., Khairunniza-Bejo, S., Abdullah, A. F., *et al*. (2020b). Application of ground-based LiDAR for analysing oil palm canopy properties on the occurrence of basal stem rot (BSR) disease. *Scientific reports*, *10*(1), 6464. https://doi.org/s41598-020-62275-6

Husin, N. A., Khairunniza-Bejo, S., Abdullah, A. F., *et al*. (2022). Multi-temporal analysis of terrestrial laser scanning data to detect basal stem rot in oil palm trees. *Precision Agriculture*, *23*(1), 101–126. https://doi.org/10.1007/s11119-021-09829-4

Husin, N. A., Khairunniza–Bejo, S., Abdullah, A. F., Kassim, M. S. M., & Ahmad, D. (2020c). Study of the oil palm crown characteristics associated with Basal Stem Rot (BSR) disease using stratification method of point cloud data. *Computers and Electronics in Agriculture*, *178*, 105810. https://doi.org/10.1016/j.compag. 2020. 105810

Karunarathna, S. C., Patabendige, N. M., Lu, W., *et al*. (2024). An in-depth study of phytopathogenic Ganoderma: Pathogenicity, advanced detection techniques, control strategies, and sustainable management. *Journal of Fungi*, 10(6), 414. https://doi.org/10.3390/jof10060414

Kent, O. W., Chun, T. W., Choo, T. L., *et al*. (2023). Early symptom detection of basal stem rot disease in oil palm trees using a deep learning approach on UAV images. *Computers and Electronics in Agriculture*, 213, 108192. https://doi.org/10.1016/j.compag.2023.108192

Kurihara, J., Koo, V. C., Guey, C. W., *et al*. (2022). Early detection of basal stem rot disease in oil palm tree using unmanned aerial vehicle-based hyperspectral imaging. *Remote Sensing*, 14(3), 799. https://doi.org/10.3390/rs14030799

Liu, X., Ghazali, K. H., Han, F., *et al*. (2021). Automatic detection of oil palm tree from UAV images based on the deep learning method. *Applied Artificial Intelligence*, 35(1), 13–24. https://doi.org/10.1080/08839514.2020.1831226

Moura, A. B., Backhouse, D., de Souza Júnior, I. T., *et al*. (2022). Soilborne pathogens. In *Subsoil constraints for crop production* (pp. 199–224). Cham: Springer International Publishing. https://doi.org/10.1007/978-3-031-00317-2_9

Siddiqui, Y., Surendran, A., Paterson, R.R.M., *et al*. (2021). Current strategies and perspectives in detection and control of basal stem rot of oil palm. *Saudi Journal of Biological Sciences*. 28, 2840–2849. https://doi.org/10.1016/j.sjbs.2021.02.016

Yarak, K., Witayangkurn, A., Kritiyutanont, K., *et al*. (2021). Oil palm tree detection and health classification on high-resolution imagery using deep learning. *Agriculture*, *11*(2), 183. https://doi.org/10.3390/agriculture11020183